Marine heatwaves confirm cloud response to warming in global climate models

Lauren Schmeisser[1]*, Thomas P. Ackerman[1], Nicholas A. Bond[1,2]

[1]Department of Atmospheric Sciences, University of Washington, Seattle, WA, USA

[2]Joint Institute for Study of the Atmosphere and Ocean, Seattle, WA, USA

Corresponding author: Lauren Schmeisser (lauren.schmeisser@gmail.com)

Key Points:

- Changes in surface longwave radiative fluxes and humidity are robustly uniform in sign during marine heatwaves across the globe
- Changes in latent heat fluxes and cloud cover dictate the geographical differences in atmosphere-ocean interactions during marine heatwaves
- Cloud changes during marine heatwaves are very similar to the cloud response to warming in global climate models

Abstract

Marine heatwaves (MHWs) are events of abnormally warm sea surface temperatures (SSTs) that can have devastating impacts on marine ecosystems and coastal economies. The evolution of these events depends partially on the local atmospheric response, and how changes in clouds and surface heat fluxes in turn affect SSTs. Understanding the role of the atmosphere in MHWs is essential for modeling and forecasting these events. Here we use satellite data from 2001-2019 to identify MHWs and anomalous atmospheric variables- including radiative heat fluxes, turbulent heat fluxes, and cloud cover- associated with these events. We find robust patterns in SST-cloud and SST-heat flux relationships that show important geographical differences in atmosphere-ocean interactions during MHWs. Because of these regional differences, we don't expect MHWs to evolve the same way in all regions. We also find that the cloud response observed during MHWs globally corresponds well with the cloud response to future warming, as identified in the Cloud Feedback Model Intercomparison Project (CFMIP) ensemble of global climate models. This suggests that MHWs can provide valuable insight to anomalous atmosphere-ocean interactions under future warming.

1 Introduction

Marine heatwaves (MHWs) are events of anomalously warm sea surface temperatures (SSTs) that exceed an upper SST threshold for an extended period of time[1,2]. MHWs have already become more frequent and more severe in the last few decades due almost entirely to warming mean ocean temperatures[3], and this trend is expected to continue with future global warming[4,5]. Although MHWs are discrete regional warming events, it is reasonable to wonder if these events offer a preview of anomalous atmosphere-ocean interactions under future warming. Here we quantify the mean local atmospheric response to MHWs, with a focus on surface heat fluxes and clouds, and evaluate whether the local responses align with changes predicted by global climate models in a warmer world.

Recent MHWs have had negative impacts on marine ecosystems and on the economies of coastal communities. Common ecological observations among recent MHWs include extreme mortality of marine species, harmful algal blooms, coral bleaching, and shifts in species ranges to cooler waters[6,7,8,9]. When fish species shift ranges during MHWs, it heavily influences the success of local fisheries, and less available catch can lead to economic devastation of fishing communities[7,8]. Understanding atmospheric perturbations that accompany past MHWs is central to understanding and modeling the physical processes driving MHWs, which will help in anticipating and minimizing future negative environmental and socioeconomic impacts during these events.

Despite the name, MHWs are not solely oceanic phenomena. They result from coupled atmosphere-ocean interactions. MHWs can be influenced by both local and non-local, large-scale atmosphere-ocean processes. In turn, MHWs can have both local and non-local atmospheric effects. Here we focus on local processes associated with MHWs and do not consider large scale climate modes or circulation changes associated with extreme SSTs. Anomalous SST patterns can be started or perpetuated locally by atypical ocean currents or processes in the ocean mixed layer, as well as atypical atmospheric processes[10,11]. In the atmosphere, the response of clouds to warm SSTs and the resulting net heat flux at the ocean surface can drive the tendency of SSTs during MHWs[11]. Understanding the changes in atmospheric processes during MHWs is important for determining regional differences in atmosphere-ocean interactions that drive MHW evolution, and for forecasting evolution of MHWs during future events.

An analysis of the atmospheric response to the 2013-2016 Northeast Pacific MHW showed substantial anomalies in cloud cover, radiative fluxes, and turbulent fluxes concurrent with the anomalously warm SSTs. During the approximately 2-year long MHW, low cloud cover decreased, downward shortwave radiative flux increased, upward and downward longwave radiative fluxes increased, and latent and sensible heat fluxes out of the ocean increased[11]. While there was a small positive net heat flux into the ocean at times during the event due to a positive SST-cloud feedback, there was a small net negative heat flux anomaly (out of the ocean, increased cooling) averaged over the lifetime of the event. The question is: does the atmosphere respond similarly during all MHW events worldwide? What can we generalize about atmospheric responses to MHWs to better understand processes that control the evolution of individual events? Does this provide insight into atmospheric adjustment to warm SSTs in a warmer future climate?

Here we: (1) detect global MHWs from 2001-2019 using satellite data and compute the additional forcing to the atmosphere during these events; (2) present local anomalous patterns in clouds and heat fluxes observed during MHW events; and (3) detail how radiative and turbulent heat flux anomalies contribute to the spatial variability in net heat flux response during MHWs. Results are compared to global climate model predictions of clouds to determine that MHWs provide an example of future anomalous atmosphere-ocean interactions.

2 Methods

The SST values used here are from the Hadley Centre Global Sea Ice and Sea Surface Temperature (HadISST) V1.1. The HadISST product uses in-situ and satellite SST measurements combined using an optimal interpolation procedure[12]. Grid boxes and timesteps in which sea ice was present were removed for this analysis. The HadISST data is available from 1871 to present, but we use 1°x1° gridded monthly means from 2001-2019 to match the availability of the radiative flux and cloud satellite data.

The surface radiative fluxes and cloud cover are from NASA's Clouds and Earth's Radiance Energy System (CERES) Energy Balanced and Filled (EBAF) Edition 4.1 satellite measurements. The CERES-EBAF Surface product is a derivative of the CERES synoptic 1° monthly means product, which calculates radiative fluxes using a 1D radiative transfer model based on inputs of temperature profiles, water vapor profiles, clouds, and other geostationary satellite observations. The data are constrained to match top of atmosphere fluxes and ocean heat storage. Detailed information on the CERES-EBAF product can be found in Kato et al. (2013) and Kato et al. (2018). CERES-EBAF data is provided on a 1°x1° grid. We use monthly means from 2001-2019. All mention of radiative fluxes here refers to fluxes at the ocean surface.

Turbulent fluxes are from the Woods Hole Oceanographic Institute (WHOI) Objectively Analyzed air-sea Fluxes (OAFlux) Project. The OAFlux product synthesizes meteorological variable estimates from various sources. The objective analysis reduces errors in individual input sources to yield an output product with minimal error. Then, the COARE 3.0 bulk flux algorithm is used to compute turbulent fluxes from the input meteorological variables. The OAFlux dataset is available over the global oceans on a 1°x1° grid and we use monthly means of latent and sensible heat fluxes from 2001-2019 to match the available time period of the CERES-EBAF data.

MHWs were detected in the HadISST dataset by first computing the climatological 95th percentile of SSTs for each month in each grid cell. Each time the mean SST in a given month exceeds the monthly 95th percentile threshold, it is flagged as a MHW in a binary file. The binary file is used to select surface heat flux and cloud cover data during MHWs. Those data are composited over all months flagged as MHWs, and averaged to yield 'MHW-averaged' variables in each grid box. The MHWs were tested for spatial and temporal coherence (i.e., are they larger than one grid cell and longer in duration than one month) by using an algorithm that clusters events that are congruent in space and/or time. Each larger/longer congruent event is given a common event label. This allows us to relate the number of MHW grid boxes to the number of global events. Given the length of the data record used here, some especially long MHWs (like the 2013-2016 NE Pacific MHW) may not be captured in their entirety by this algorithm, which necessarily only detects 5% of months as MHWs. In this sense, we can view this analysis as capturing the MHW months with the highest magnitude SST anomalies (as opposed to capturing all MHW months). Lowering the detection threshold to a 90th percentile threshold helps address this issue of including entire MHWs; however, a sensitivity analysis showed that changing the threshold did not significantly alter results presented here.

To help interpret any regional differences in average surface heat fluxes or cloud cover during marine heatwaves compared to average conditions, it is useful to know if the atmosphere experiences similar regional forcing due to a change in SSTs during MHWs. We assume that the forcing from the sea surface to the atmosphere can be quantified as the upwelling longwave radiative flux, computed by the Stefan-Boltzmann equation:

$$LW = \epsilon\sigma T^4 \qquad [1]$$

We can quantify the difference in forcing by the ocean surface to the atmosphere between normal and marine heatwave conditions by differentiating the Stefan-Boltzmann equation and rearranging:

$$\frac{dLW}{dT} = 4\epsilon\, \sigma\bar{T}^3 \qquad [2]$$

$$dLW = 4\epsilon\, \sigma\bar{T}^3(T' - \bar{T}) \qquad [3]$$

where LW is the upward longwave radiative flux at the ocean surface, σ is the Stefan-Boltzmann constant, ϵ is the emissivity (which we assume is unity at the ocean surface and will be dropped in further equations), $\bar{T}$ is the mean SST, and *T'* is the MHW SST threshold at the 95th percentile. The equation can be rearranged and reduced to a fractional representation to yield:

$$\frac{dLW}{\sigma\bar{T}^4} = 4\ \frac{(T' - \bar{T})}{\bar{T}} \qquad [4]$$

This equation can be multiplied by 100 and used to analyze the percentage change in forcing during MHWs in different regions around the world. The hypothesis is that, if there are differences in forcing during a MHW warming, the atmosphere will show larger anomalies in regions where the forcing from SST changes is also larger.

3 Results

3.1 MHW Detection & Forcing during MHWs

The MHW detection algorithm identified 16,550 spatially and/or temporally congruent MHW events in the 18-year SST dataset. While this number appears large, recall there are approximately 45,360 1°x1° oceanic grid cells. In 18 years, each grid cell experiences on average 11 months (~5% of an 18-year data record) of MHW conditions, which means our algorithm has detected a reasonable number of clustered MHW events, given the 95th percentile detection threshold. For all MHWs identified across the globe, the average SST anomaly for all events was 0.8 °C.

Figure 1 shows the change in forcing due to anomalously warm SSTs during MHW conditions as computed in Equation 4, averaged over all seasons. The forcing change due to a warmer SST during MHWs is not uniform globally. Areas of strong forcing are evident in regions such as the Northeast Pacific, Northwest Atlantic, central and eastern tropical Pacific, and the Southwest Atlantic. While Figure 1 is computed using data from 2001-2018, and thus the 95th percentile thresholds used in the calculation may be influenced by recent large and severe MHWs, the same calculation using the full HadISST dataset (1870-2018) yields nearly the same spatial pattern (though magnitudes of percentage forcing change are larger, see Figure S1 in supplemental material). The fact that the larger forcing changes observed in some regions compared to others are robust across a long dataset highlights unique atmosphere-ocean interactions occurring in these regions.

The magnitude of the average SST anomaly during MHWs (Figure 2a) matches the pattern of forcing change (Figure 1), as expected. As we show, regions that experience a greater percentage change in forcing also experience larger anomalies in some atmospheric variables during MHWs.

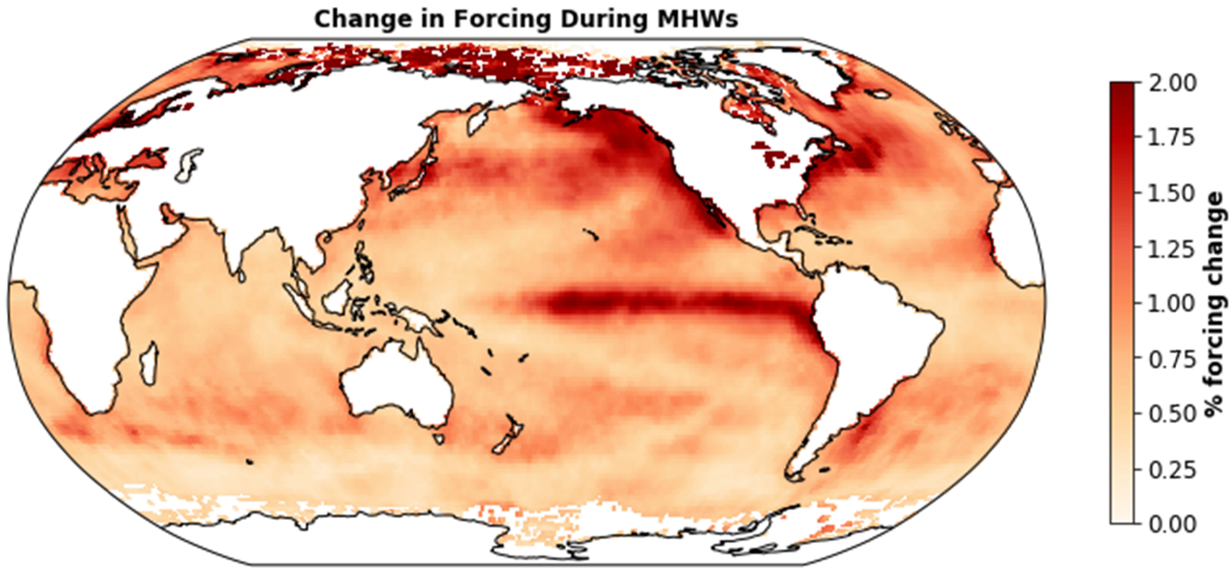

Figure 1. Percentage change in forcing [W/m^2] from upward longwave radiative flux at the surface driven by warming of SSTs from climatological SSTs to MHW threshold, averaged over time period 2001-2019

3.2 Atmospheric perturbations during MHWs

Our analysis shows that there are robust atmospheric perturbations associated with MHWs. Upward longwave radiative flux increases during MHWs globally, as dictated by the Stefan-Boltzmann law (Figure 2c). Upward longwave radiative flux anomalies are highest in regions that experienced the highest SST anomalies during MHWs (Figure 2a), particularly in the NE Pacific, eastern tropical Pacific, and northwest Atlantic. Downward longwave radiative flux also increases almost everywhere worldwide (Figure 2d), which is largely dictated by ubiquitous and concurrent increases in air temperature (not shown) and humidity (Figure 2b). Cloud changes seem to have a smaller effect on this downward longwave signal.

During MHWs, low clouds decrease nearly everywhere, with the exception of a large area in the northwest Pacific, high latitudes in the Arctic and Antarctic, and scattered local coastal regions (Figure 3a). High cloud generally increases everywhere (Figure 3b). The combination of these two opposing signals results in high spatial variability in the total cloud cover response (Figure 3c). The cloud response is one of the key differences between atmospheric patterns during MHWs in the tropics compared to the midlatitudes. Large scale patterns show an increase in total cloud cover during MHWs in the tropics, a decrease in total cloud cover during MHWs in the subtropics and midlatitudes, and an increase in total cloud cover in the very high latitudes (Figure 3c).

The cloud response dictates the downward shortwave anomalies observed during MHWs and, thus, there is large spatial variability in the shortwave flux anomalies as well. Downward shortwave radiative fluxes decrease in the tropics, increase in the subtropics and midlatitudes, and decrease in the high latitudes during MHWs (Figure 2e).

Latent heat flux anomalies during MHWs are regionally variable, with the largest anomalies (positive out of the ocean) in the tropical Pacific, as well as in western boundary current regions (e.g., the Kuroshio current in the northwest Pacific and the Gulf Stream current in the northwest Atlantic) (Figure 2g). Throughout large areas in the subtropics and midlatitudes, latent heat flux anomalies are small and negative (indicating less cooling by latent heat fluxes). Sensible heat fluxes are small compared to other flux terms everywhere (Figure 2h) except at very high latitudes, where our confidence in the data is lower due to interference by sea ice and challenges with satellite retrievals.

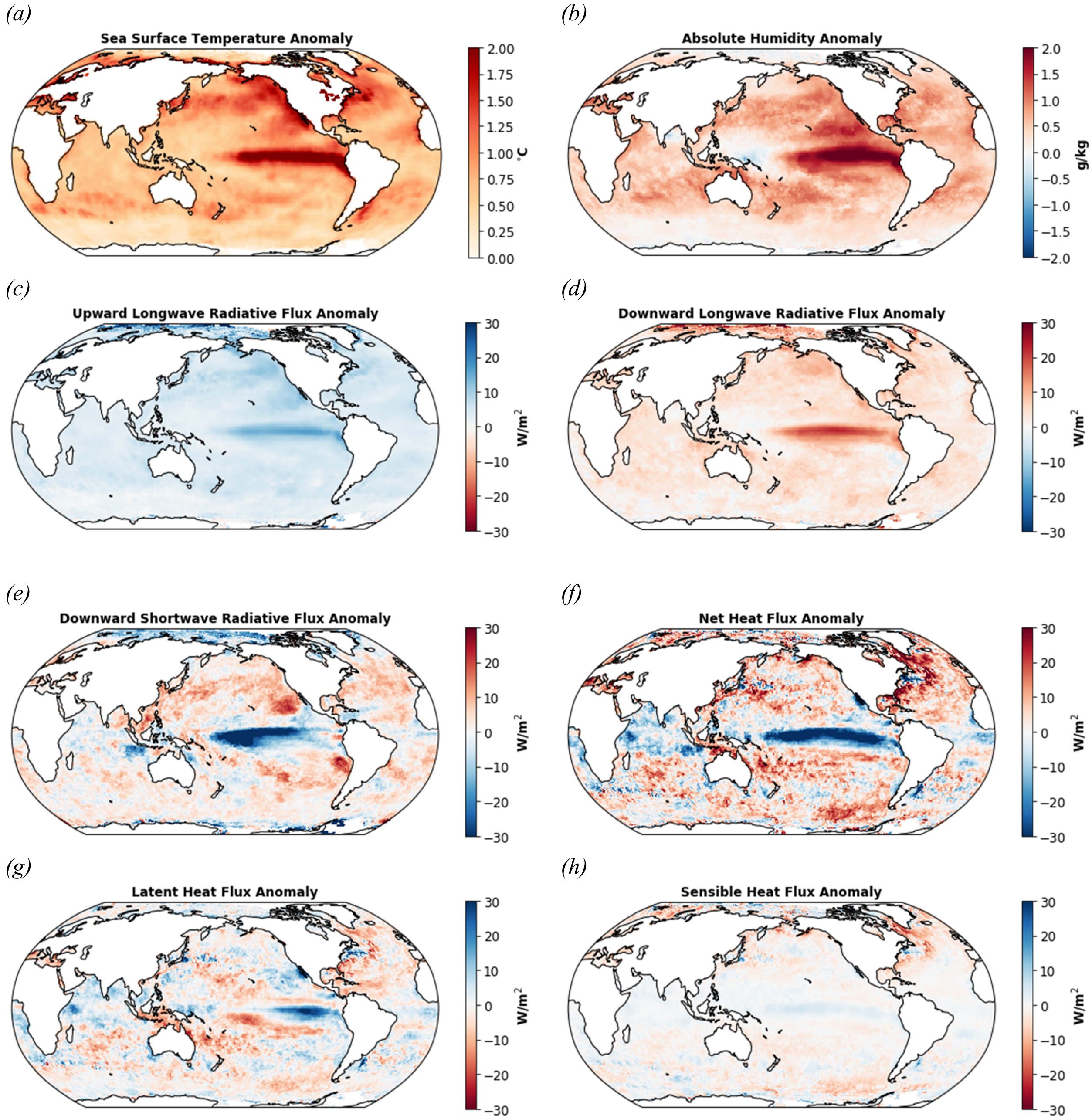

Figure 2. Atmospheric variable anomalies composited and averaged during MHW events: (a) SST anomalies (°C), (b) 2 m absolute humidity anomalies (g/kg), (c) upward longwave radiative flux anomalies at the surface (W/m^2) (positive is up), (d) downward longwave radiative flux anomalies at the surface (positive is down), (e) downward shortwave radiative flux anomalies at the surface (positive is down), (f) net heat flux anomalies (W/m^2), (g) latent heat flux anomalies (W/m^2), and (h) sensible heat flux anomalies (W/m^2) (positive is up).

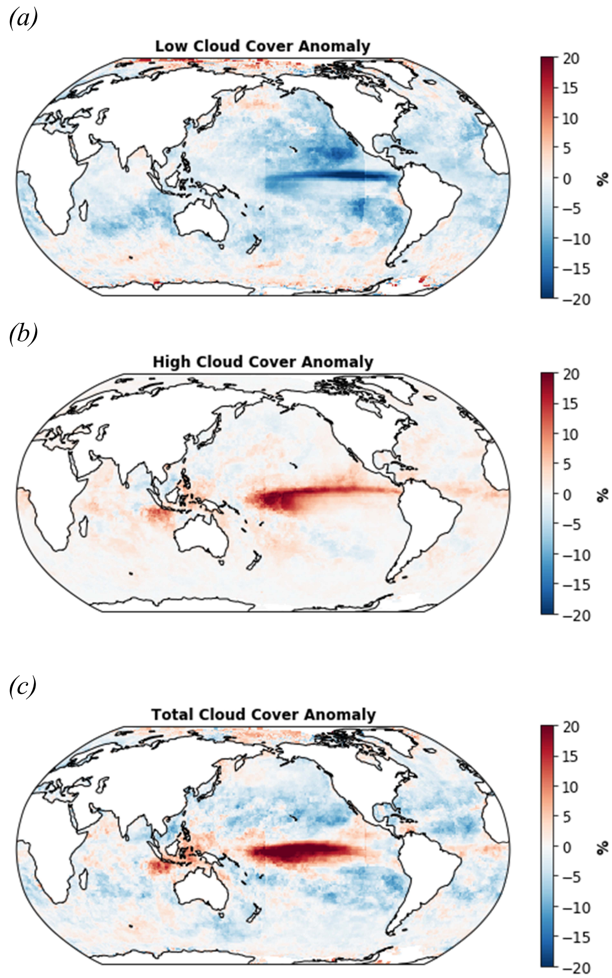

Figure 3. Cloud cover anomalies composited and averaged during MHW events: (a) low cloud cover anomalies (%) (b) non-low cloud cover anomalies (%), and (c) total cloud cover anomalies (%)

3.2 Surface net heat flux changes during MHWs

The surface net heat flux during MHWs measures the atmospheric contribution to SST tendency in the ocean mixed layer. The surface net heat flux anomaly shows large spatial variability during MHWs, indicating that the effect of the atmosphere on SSTs during MHWs is not globally uniform.

The MHW-averaged net heat flux anomaly tends to be positive (into the ocean) in the subtropics and midlatitudes, and negative (out of the ocean) in the tropics (Figure 2f). In general terms, the atmospheric response to warm SSTs contributes to the SST tendency by enhancing warming in the subtropics and midlatitudes with a positive net heat flux anomaly, and damping warming in the tropics with a negative net het flux anomaly. There are some smaller regions that are exceptions (e.g., off Baja California and in the northwest Atlantic).

Comparing the contour plots of net heat flux anomaly (Figure 2h) and downward shortwave radiative flux anomaly (Figure 2e) suggests that the change in shortwave radiative flux at the surface caused by the cloud response during MHWs is largely driving the regional variability in net heat fluxes. Anomalies in latent heat fluxes also contribute substantially, particularly in western boundary current regions and the tropics. Since upward and downward longwave radiative flux anomalies have robustly similar signs (and, to a lesser extent, similar magnitudes) during MHWs in all regions of the globe (Figures 2c,d), they are not contributing much to the spatial structure of the net heat flux anomaly.

We can quantify the extent to which heat flux components (i.e., downward/upward longwave, downward/upward shortwave, latent, and sensible fluxes) contribute to regional variations in net heat flux anomaly by computing the percentage contribution of each heat flux component anomaly to the total net heat flux anomaly during MHWs in each grid box. We do this by dividing the absolute value of each individual net heat flux component anomaly by the sum of the absolute value of all net heat flux component anomalies. Results of this calculation are shown in Figure 4. In many places, downward shortwave radiative flux anomalies (Figure 4d) and latent heat flux anomalies (Figure 4e) are the dominant contributors to net heat flux anomalies during MHWs. The fact that latent heat fluxes account for 20-40% of the anomalous net heat flux response during MHWs is particularly notable since under climatological conditions, latent heat fluxes are a much smaller contributor to net heat fluxes (5-10%, not shown).

Downward and upward longwave radiative flux anomalies contribute secondarily to the net heat flux anomaly spatial variation in most regions (Figures 4a,b). Sensible heat flux anomalies and upward shortwave radiative flux anomalies only contribute substantially in very high latitudes where sea ice is often present (Figures 4c,f).

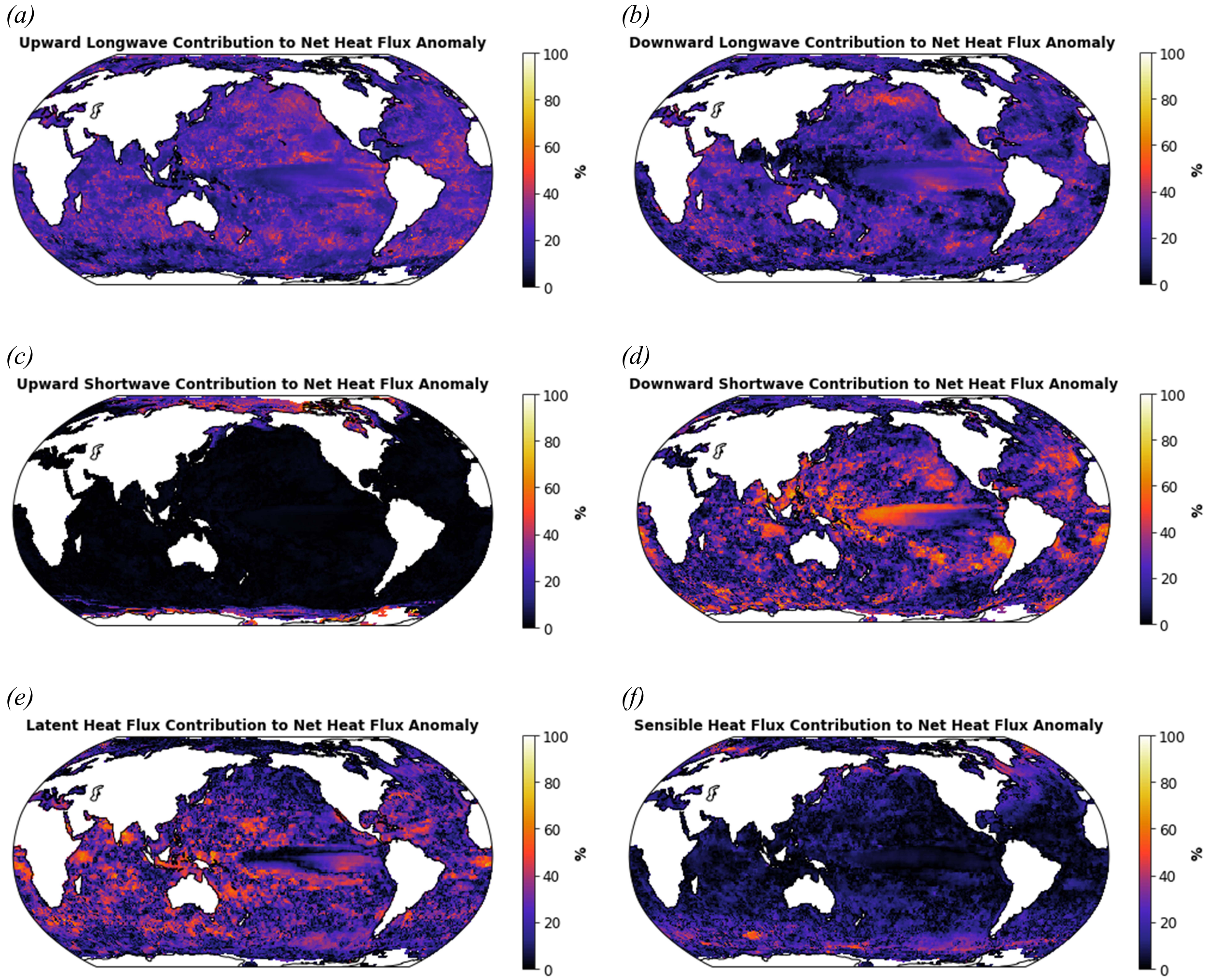

Figure 4. Percentage contribution of (a) upward longwave radiative flux anomaly, (b) downward longwave radiative flux anomaly, (c) upward shortwave radiative flux anomaly, (d) downward shortwave radiative flux anomaly, (e) latent heat flux anomaly, and (f) sensible heat flux anomaly to the MHW-averaged net heat flux anomaly.

4 Summary & Discussion

4.1 Changes in forcing from the ocean to the atmosphere during MHWs

Our analysis shows that anomalous local forcing from the sea surface to the atmosphere during MHWs is regionally variable. Regions experiencing the highest SST anomalies and, thus, upward radiative flux anomalies during MHWs were also the regions that had the highest change in percentage forcing from the ocean surface to the atmosphere. This isn't an inevitable conclusion, given that the change in forcing is normalized by the average temperature of a region. This indicates that certain regions are prone to experiencing especially warm SST anomalies relative to other regions with similar average temperatures, and as a consequence, the forcing on the atmosphere from anomalous SSTs during MHWs is larger in these regions.

Furthermore, ocean-atmosphere interactions have an amplified response in these places. For some atmospheric variables (downward longwave radiative flux, cloud cover and latent heat fluxes), the larger forcing may be associated with larger atmospheric anomalies. The implication is that the world's oceans are not uniform in response to MHWs, and our analyses and modeling efforts should reflect the heterogeneity in regional evolution of these extreme events.

4.2 Atmospheric patterns during MHWs

Our results capture MHW months with only the most extreme SSTs; they represent only the highest 5% of SST anomalies during the data period. In some extreme cases when the MHW persists for many months of years, like that of the 2013-2016 NE Pacific MHW, the entire event is not captured in this analysis since the duration is longer than could be captured by the MHW detection algorithm given the length of the data record. (For analyses of individual events with longer duration, the threshold for MHW detection can be reduced to, say, the 90^{th} percentile or below, in order to analyze the full consecutive event; alternatively, the detection algorithm can be altered so that time periods in which SSTs drop below the threshold can be included in the event if the anomalies are bookended on both sides by MHW conditions). Throughout the evolution of an entire MHW, the atmospheric patterns may vary. For example, in the 2013-2016 NE Pacific MHW, the average net heat flux anomaly over the duration of the event was net negative[11]. However, the analysis here shows the net heat flux anomaly in that same region is net positive. A careful look at the time series of net heat flux anomalies during the event indicates that during the time periods of most intense SST anomalies (also captured in this analysis), the net heat flux anomaly is indeed positive. However, averaging over the lifetime of the MHW yields a negative net heat flux anomaly, as this includes months when the SSTs were cooling back to below the MHW threshold. While composited MHW results are useful, a careful time series analysis of individual events is also crucial in understanding dynamics that are at play throughout the build-up, duration, and decay of the MHW. The dynamics during each phase will be different and not necessarily the same as the processes represented in event-composited results.

It is also prudent to note that this analysis does not consider non-local downstream impacts of extreme SSTs associated with MHWs. One could imagine that a perturbation in the underlying SST would not only have a local impact, but also could be carried by the atmosphere downstream and ultimately influence surface heat fluxes and cloud cover. These non-local responses could depend on the spatial extent of the MHW; for example, if a MHW is large enough, the atmosphere may more fully equilibrate to the SST anomalies. While not addressed here, this is an important area of future research.

Regional patterns in MHW-averaged cloud anomalies presented here generally align well with SST-cloud relationships published in the literature. As SSTs increase during a MHW, low clouds decrease almost everywhere[15,16,17,18]. One notable exception is the northwest Pacific (Sea of Okhotsk and Bering Sea regions), for which the literature on SST-cloud relationships is sparse, though it is reasonable to assume this area is intermittently affected by sea ice and/or cold air outbreaks from the Siberian region that could influence clouds. The Southern Ocean also experiences increases in low cloud in some areas, which could be attributed to sea ice interaction or poor data quality at high latitudes. We show that high clouds generally increase everywhere during MHWs. This is expected given the SST-high cloud relationships outlined in the literature which suggest deep convection generally increases with warming ocean waters[19,20]. This is especially apparent in our high cloud results in the central and eastern Pacific, when warm waters typically associated with El Niño and a shift in the Walker circulation bring deep convection and precipitation to these areas. Increases in high cloud cover in the subtropics or midlatitudes associated with warm SSTs[19,20] or MHWs[11,21] have been observed by many other studies as well. Our MHW-composited cloud anomaly results show that, even at the tail end of the SST distribution (MHW events), our understanding of cloud behavior under warm SSTs is consistent with the observations.

The influence of the El Niño-Southern Oscillation is apparent in the tropical Pacific in many of the figures presented. We note that a strong El Niño event can technically be classified as a MHW in the east and central equatorial Pacific, so El Niño events are rightly included in the analysis, since we are interested to see how extreme SSTs influence the atmosphere. While the driving forces of El Niño-related MHWs could certainly be different than the driving forces of other MHWs globally, we are not concerned here with what drives the spin-up of the MHW; rather, we are focused on the overlying atmospheric anomalies associated with warm SST events. In fact, including El Niño-influenced events provides an excellent confirmation of our results. The increased convection in the central and eastern tropical Pacific, represented by decreased low cloud and increased high cloud fractional coverages, aligns with our expectations of El Niño behavior. Additionally, the increase in humidity in the eastern and tropical Pacific aligns with the changes in the Walker circulation during El Niño events.

In the case of downward longwave radiative flux, a near universal increase during MHWs is somewhat surprising given the spatial differences in cloud changes regionally. Since downward longwave radiative flux is determined mainly by air temperature, humidity levels, and cloud cover, regional variability in the magnitude of cloud cover anomalies during MHWs might be expected to yield regional variability in downward longwave radiative flux anomalies at the surface. Rather, the widespread increases in air temperature and humidity dominate the downward longwave response. Cloud changes are of secondary importance on downward longwave radiative flux anomalies during MHWs. These results provide observational evidence during natural warming events that support the theory that downward longwave radiative flux is largely set by surface temperatures and the resulting turbulent fluxes that warm and moisten the overlying atmosphere; cloud changes make a much smaller contribution[22].

It is worth mentioning that the seasonal dependence of these results is not analyzed here, as the relatively short time series of MHW events does not allow for sufficient data points in each season to provide robust results. However, there is good reason to think that these results are seasonally dependent. For example, outside of the tropics when the oceanic mixed layer is shallow, it may be easier to warm the ocean water to MHW levels and thus a disproportionate fraction of MHWs could occur in the warm season. Additionally, climatological cloud cover differs from season to season in many parts of the world, so cloud response, and more importantly- the impact of that cloud response on net heat flux at the ocean surface- could depend heavily on the season. Future work analyzing seasonal dependence of the atmospheric response to MHWs using longer datasets should be prioritized.

4.3 Implications

There are two important implications of this analysis. First, we show that the role of the atmosphere in MHWs is regionally variable and, because of these regional differences in atmosphere-ocean interactions, we do not expect MHWs to evolve similarly in all regions.

Second, we argue that the MHW-averaged atmospheric responses shown here are similar to global climate model predictions of those atmospheric variables in a warmer world, suggesting that MHWs provide a observational surrogate of what surface flux and atmospheric changes will look like in a warmer world. The results of our analysis show that some atmospheric variables have a similar and robust local response to MHWs in all regions globally, while other atmospheric variables behave differently in the tropics, subtropics, and midlatitudes. These differences combine to produce spatial variability in the net heat flux response during MHWs. The net heat flux during MHWs encompasses the atmospheric effects on SST tendency; consequently, the local atmospheric contribution to MHWs is regionally variable.

Atmospheric variables like downward and upward longwave radiative fluxes at the surface, low cloud cover, high cloud cover, and humidity anomalies are robustly uniform in sign during MHWs in nearly all regions. But atmospheric variables like latent heat flux, total cloud cover, and downward shortwave radiative flux anomalies show large regional differences in sign. It is the latter variables that drive the global spatial differences in net heat flux response at the surface during MHWs. Generally speaking, the atmosphere tends to cool SSTs through a negative surface net heat flux anomaly during MHWs in the tropics; the opposite is the case during MHWs in the subtropics and midlatitudes. Differences in tropical versus subtropical vs. midlatitude atmosphere-ocean interactions are largely dictated by cloud response and latent heat fluxes, which emphasizes the importance of understanding clouds and latent heat fluxes to properly model the coupled climate system.

Average SSTs in most ocean basins will warm 1°C above 1986-2006 historical averages by the end of the century in an RCP4.5 scenario, and by 2050 in an RCP8.5 scenario[23]. The SST anomalies during MHWs presented here average about 0.8 °C, and thus are a conservative representation of the future ocean conditions under global warming. The global response of total cloud cover to MHWs in our data set closely resembles the global response of total cloud cover per degree warming in the global climate model ensemble mean from the Cloud Feedback Model Intercomparison Project (CFMIP; Zelinka et al., 2012, Figure 1). Models and observational data from MHWs both show an increase in total cloud cover over the tropical oceans, a decrease in the subtropics and midlatitudes, and an increase in the high latitudes. Regional changes in low cloud and non-low cloud fraction (which make up changes in total cloud fraction) during MHWs are also consistent with those from global climate model ensemble means (Mark Zelinka, personal communication).

We do not claim MHWs are exact replicas of future ocean conditions. For example, large-scale SST gradients that exist currently between MHW regions and neighboring non-MHW regions will either not be present or very significantly reduced when future SST warming happens on a global scale. Nevertheless, MHW events provide valuable insight into the potential atmospheric response to future warming of SSTs. It is a reasonable hypothesis that radiative fluxes, turbulent fluxes, clouds, and humidity will respond similarly to future warm SSTs as observed in the MHWs analyzed here. Furthermore, MHWs can help validate atmospheric response to warming SSTs in global climate models. We show that cloud response is a key factor in determining the net het flux response to MHWs and, thus, the atmospheric contribution to SST tendency during MHWs. Correctly modeling clouds in global climate models is fundamental to properly representing atmosphere-ocean interactions and net heat fluxes in global climate models; therefore, it is encouraging to see the consistency between the results in this MHW analysis and model ensemble means.

Acknowledgements

Sea surface temperatures from the HadISST dataset are available from the Met Office Hadley Centre website https://www.metoffice.gov.uk/hadobs/hadisst/. CERES-EBAF data are provided by NASA and available for download here: https://ceres.larc.nasa.gov/products.php?product=EBAF-Surface. Turbulent heat fluxes were provided by the WHOI OAFlux project (http://oaflux.whoi.edu) and funded by the NOAA Climate Observations and Monitoring (COM) program.The lead author would like to thank the Joint Institute for Study of the Atmosphere and Ocean graduate fellowship program, in conjunction with the University of Washington College of the Environment, for partial funding of this work. The authors would like to acknowledge Dr. Mark Zelinka for his helpful insights on cloud response in global climate models. The authors have no real or perceived financial conflicts of interest.

References

Bellomo, K., Clement, A. C., Mauritsen, T., Rädel, G., & Stevens, B. (2015), The influence of cloud feedbacks on equatorial Atlantic variability. *Journal of Climate*, *28*(7), 2725-2744. doi:10.1175/JCLI-D-14-00495.1

Cavole, L. M., Demko, A. M., Diner, R. E., Giddings, A., Koester, I., Pagniello, C. M. L. S., Paulsen, M.-L., Ramirez-Valdez, A., Schwenck, S. M., Yen, N. K., Zill, M. E., & Franks, P. J. S. (2016), Biological impacts of the 2013-2015 warm-water anomaly in the Northeast Pacific: Winners, losers and the future. *Oceanography,* 29(2), 273-285, doi:10.5670/oceanog.2016.32

Clement, A. C., Burgman, R., & Norris, J. R. (2009). Observational and model evidence for positive low-level cloud feedback. *Science*, *325*(5939), 460-464, doi:10.1126/science.1171255

De Szoeke, S. P., Verlinden, K. L., Yuter, S. E., & Mechem, D. B. (2016). The time scales of variability of marine low clouds. *Journal of Climate*, *29*(18), 6463-6481, doi:10.1175/JCLI-D-15-0460.1

Frölicher, T. L., & Laufkötter, C. (2018). Emerging risks from marine heat waves. *Nature communications*, *9*(1), 650, doi:10.1038/s41467-018-03163-6

Frölicher, T. L., Fischer, E. M., & Gruber, N. (2018). Marine heatwaves under global warming. *Nature*, *560*(7718), 360-364, doi: 10.1038/s41586-018-0383-9

Hobday, A. J., Alexander, L. V., Perkins, S. E., Smale, D. A., Straub, S. C., Oliver, E. C. J., Benthuysen, J. A., Burrows, M. T., Donat, M. G., Feng, M., Holbrook, N. J., Moore, P. J., Scannell, H. A., Sen Gupta, A., & Wernberg, T. (2016). A hierarchical approach to defining marine heatwaves. *Progress in Oceanography*, 141, 227-238, doi:10.1016/j.pocean.2015.12.014

Hobday, A. J., Oliver, E. C. J, Sen Gupta, A., Benthuysen, J. A., Burrows, M. T., Donat, M. G., Holbrook, N. J., Moore, P. J., Thomsen, M. S., Wernberg, T., & Smale, D. A. (2018). Categorizing and naming marine heatwaves. *Oceanography*, 31(2), doi:10.5670/oceanog.2018.205

Holbrook, N. J., Scannell, H. A., Gupta, A. S., Benthuysen, J. A., Feng, M., Oliver, E. C., Alexander, L. V., Burrows, M. T., Donat, M. G., Hobday, A. J., Moore, P. J., Perkins-Kirkpatrick, S. E., Smale, D. A., Straub, S. C., & Wernberg, T. (2019). A global assessment of marine heatwaves and their drivers. *Nature communications*, *10*(1), 1-13, doi:10.1038/s41467-019-10206-z

Hoegh-Guldberg, O., R. Cai, E.S. Poloczanska, P.G. Brewer, S. Sundby, K. Hilmi, V.J. Fabry, and S. Jung, 2014: The Ocean. In: *Climate Change 2014: Impacts, Adaptation, and Vulnerability. Part B: Regional Aspects. Contribution of Working Group II to the Fifth Assessment Report of the Intergovernmental Panel on Climate Change* [Barros, V.R., C.B. Field, D.J. Dokken, M.D. Mastrandrea, K.J. Mach, T.E. Bilir, M. Chatterjee, K.L. Ebi, Y.O. Estrada, R.C. Genova, B. Girma, E.S. Kissel, A.N. Levy, S. MacCracken, P.R. Mastrandrea, and L.L. White (eds.)]. Cambridge University Press, Cambridge, United Kingdom and New York, NY, USA, pp. 1655-1731.

Kato, S., Loeb, N. G., Rose, F. G., Doelling, D. R., Rutan, D. A., Caldwell, T. E., ... & Weller, R. A. (2013). Surface irradiances consistent with CERES-derived top-of-atmosphere shortwave and longwave irradiances. *Journal of Climate*, *26*(9), 2719-2740, doi:10.1175/JCLI-D-12-00436.1

Kato, S., Rose, F. G., Rutan, D. A., Thorsen, T. J., Loeb, N. G., Doelling, D. R., Huang, X., Smith, W. L., Su, W., & Ham, S. (2018). Surface Irradiances of Edition 4.0 Clouds and the Earth's Radiant Energy System (CERES) Energy Balanced and Filled (EBAF) Data Product. *Journal of Climate*, 31, 4501-4527, doi:10.1175/JCLI-D-0523.1

Klein, S. A., Hartmann, D. L., & Norris, J. R (1995). On the relationships among low-cloud structure, sea surface temperature, and atmospheric circulations in the summertime northeast Pacific. *Journal of Climate,* 8, 1140-1155, doi:10.1175/15200442(1995)008<1140:OTRALC->2.0.CO;2

Le Nohaïc, M., Ross, C. L., Cornwall, C. E., Comeau, S., Lowe, R., McCulloch, M. T., & Schoepf, V. (2017). Marine heatwave causes unprecedented regional mass bleaching of thermally resistant corals in northwestern Australia. *Nature Scientific Reports*, 7(14999), doi:10.1038/s41598-017-14794-y

McCabe, R. M., Hickey, B. M., Kudela, R. M., Lefebvre, K. A., Adams, N. G., Bill, B. D., Gulland, F. M. D., Thomson, R. E., Cochlan, W. P., & Trainer, V. L. (2016). An unprecedented coastwide toxic algal bloom linked to anomalous ocean conditions, *Geophysical Research Letters*, 43(10), 10366-10376, doi:10.1002/2016GL070023

Myers, T. A., Mechoso, C. R., Cesana, G. V., DeFlorio, M. J., & Waliser, D. E (2018). Cloud feedback key to marine heatwaves off Baja California. *Geophysical Research Letters* 45, 4345-4352, doi:10.1029/2018GL078242

Oliver, E. C. J., Donat, M. G., Burrows, M. T., Moore, P. J, Smale, D. A., Alexander, L. V., et al. (2018). Longer and more frequent marine heatwaves over the past century, *Nature Communications,* 9(1), 1324, doi:10.1038/s41467-018-03732-9

Piatt, J. F., Parrish, J. K., Renner, H. M., Schoen, S. K., Jones, T. T., Arimitsu, M. L., Kuletz, K. J., Bodenstein, B., García-Reyes, M., Duerr, R. S., Corcoran, R. M., Kaler, R. S. A., McChesney, G. J., Golightly, R. T., Coletti, H. A., Suryan, R. M., Burgess, H. K., Lindsey, J., Lindquist, K., Warzybok, P. M., Jahncke, J., Roletto, J. & Sydeman, W. J. (2020). Extreme mortality and reproductive failure of common murres resulting from the northeast Pacific marine heatwave of 2014-2016. *PLoS One*, *15*(1), e0226087, doi: 10.1371/journal.pone.0226087

Ramanthan, V. & Collins, W. (1991). Thermodynamic regulation of ocean warming by cirrus clouds deduced from observations of the 1987 El Niño. *Nature,* 353, 737-740, doi: 10.1038/351027a0

Rayner, N. A., Parker, D. E., Horton, E. B., Folland, C. K., Alexander, L. V., Rowell, D. P., Kent, E. C., & Kaplan, A. (2003) Global analyses of sea surface temperature, sea ice, and night marine air temperature since the late nineteenth century J. Geophys. Res.Vol. 108, No. D14, 4407, doi:10.1029/2002JD002670

Schmeisser, L., Bond, N. A., Siedlecki, S. A., & Ackerman, T. P. (2019). The Role of Clouds and Surface Heat Fluxes in the Maintenance of the 2013–2016 Northeast Pacific Marine Heatwave. *Journal of Geophysical Research: Atmospheres*, *124*(20), 10772-10783, doi: 10.1029/2019JD030780

Vargas Zeppetello, L. R., Donohoe, A., & Battisti, D. S. (2019). Does Surface Temperature Respond to or Determine Downwelling Longwave Radiation?. *Geophysical Research Letters*, *46*(5), 2781-2789, doi:10.1029/2019GL082220

Zhang, C. (1993). Large-scale variability of atmospheric deep convection in relation to sea surface temperature in the tropics. *Journal of Climate*, *6*(10), 1898-1913, doi:10.1175/1520-0442(1993)006<1898:LSVOAD>2.0.CO;2

Zelinka, M. D., Klein, S. A., & Hartmann, D. L. (2012). Computing and partitioning cloud feedbacks using cloud property histograms. Part II: Attribution to changes in cloud amount, altitude, and optical depth. *Journal of Climate,* 25(11), 3736-3754, doi:10.1175/JCLI-D-11-00249.1